Low-temperature, diagenetic serpentinization of peridotite clasts in lower Miocene marine conglomerates, Torino Hill, NW Italy

Low-temperature, diagenetic serpentinization of peridotite clasts in lower Miocene marine conglomerates (Torino Hill, NW Italy)

Barale L.[1,2], Petriglieri J.R.[3,2], Botta S.[3], Piana F.[1,2]

1: National Research Council of Italy, Institute of Geosciences and Earth Resources, Torino.

2: University of Torino, Interdepartmental Centre "G. Scansetti" for Studies on Asbestos and Other Toxic Particulates.

3: University of Torino, Department of Chemistry.

Abstract

Peridotite clasts in a marine Miocene conglomerate from the Torino Hill (NW Italy) are characterised by an isopachous serpentinized external rim (4–12 mm thick) made up of lizardite, surrounding a non-serpentinized peridotite core. This peculiar structure indicates a diagenetic, post-depositional serpentinization of the peridotite clasts. The conglomerate is cemented by a rim of lizardite, followed by Mg-calcite and Ca-dolomite spar. The burial history of the host sedimentary succession indicates that serpentinization and precipitation of lizardite cements occurred at very low temperature (max. 50–60°C). This is the first reported case of diagenetic, very low temperature serpentinization affecting ultramafite clasts in sedimentary successions.

Keywords: low-*T* serpentinization, lizardite, peridotite, marine diagenesis, Tertiary Piemonte Basin

1. Introduction

Serpentinization is one of the most important and widely studied geological processes on Earth and can occur in a variety of geodynamic environments (e.g., Guillot and Hattori 2013, with refs.). Of the three most common serpentine minerals, i.e. antigorite, lizardite and chrysotile, only the latter two can form at low temperature (e.g., Evans, 2004). Low-*T* serpentinization is a well-known process in oceanic settings, where it results from seawater

circulation in ultramafic mantle rocks (e.g., Agrinier et al., 1996; Früh-Green et al., 2004; Cannat et al., 2010), as well as in continental settings, where meteoric water circulation promotes serpentinization of obducted (meta-)ophiolite sequences (e.g., Barnes et al., 1978; Schrenk et al., 2013; Sánchez-Murillo et al., 2014; Etiope, 2017). Fryer and Mottl (1992) also hinted at the possibility of low-temperature, seawater-related serpentinization of ultramafic clastic material blanketing serpentinite seamounts of the Mariana forearc region. On the other hand, diagenetic serpentinization of ultramafite clasts in sedimentary deposits of non-oceanic settings was only once reported in the literature (Cashman and Whetten, 1976).

Here we report a case of very low-*T* (<<100°C), marine diagenetic serpentinization of peridotite pebbles and cobbles within the early Miocene Bric Palouch Conglomerate (Tertiary Piemonte Basin, NW Italy). Serpentinization resulted in the development of a lizardite serpentinite rim, up to 10–12 mm thick, surrounding a more or less preserved lherzolite core.

2. Geological setting

The Aquitanian Bric Palouch Conglomerate (BPC) lies in the upper part of the Antognola Formation in the southern sector of the Torino Hill (TH), a tectono-sedimentary sub-domain of the Tertiary Piemonte Basin (TPB) with an upper Eocene–Messinian, mainly terrigenous succession (Festa et al., 2009; Piana et al., 2017, with refs.; Fig. 1a). The Antognola Formation (Chattian–Aquitanian) consists of hemipelagic silty marl with sandstone layers. In the southern part of the TH, this unit is 400–500 m thick, contains lenticular conglomerate bodies interpreted as infillings of submarine canyons, and is followed by 1000–1200 m of Burdigalian–Messinian TPB sediments and 200–300 m of Pliocene deposits (Polino et al., 1991; Festa et al., 2009).

The BPC differs from the other conglomerate bodies of the Antognola Formation due to this peculiar composition, being almost entirely composed of meta-ophiolite clasts: serpentinite prevails, accompanied by metagabbro, radiolarite and marble (Elter et al., 1966; Compagnoni and Forno, 1992; Festa et al., 2009). Sacco (1936) also cited rare peridotite pebbles and noted that the BPC is "*cemented by a kind of serpentinous and silico-magnesiac paste*" (Sacco, 1936, p. 94).

3. Materials and methods

Samples were collected in the Bric Palouch abandoned quarry (45°04'19.3"N; 7°47'22.2"E) from both outcrops (PCH1, 2, 9) and quarry scree (PCH10, 11) (Fig. 1b). Petrographic observations were coupled with micro-Raman spectroscopy to achieve an univocal identification of serpentines (e.g., Rinaudo et al., 2003; Petriglieri et al., 2015; Compagnoni et al., 2021). The mineralogy of fine-grained aggregates unresolvable with the above methods was determined by X-ray powder diffraction (XRPD). Mineral compositions were determined by SEM–EDS. The analytical details are given in Supplementary File 1.

4. The Bric Palouch Conglomerate

4.1. General features

The Bric Palouch Conglomerate (BPC) forms a lenticular body with a maximum thickness of 40–50 metres and a lateral extension of a few hundred metres (Fig.1b). The BPC has an ill-defined, metre thick bedding (Fig. 2a) and shows a dark green to blackish colour on fresh fractures passing to reddish brown on weathered surfaces. BPC clasts are generally well rounded and vary in size from a few millimetres to several decimetres.

About 95% of the BPC clasts consist of (meta-)ultrabasite, including serpentinite, serpentine-schist, and peridotite (Fig. 2b). The remaining clasts are composed of: metagabbro (locally rodingitised), metabasite, (meta-)radiolarite, micritic limestone (commonly with abundant carbonate veins), dolomitic limestone, marble, calc-schist, and very rare reddish quartz porphyry. Rare bioclasts occur (solitary corals, bivalve fragments).

The BPC is more cemented with respect to the surrounding sedimentary succession and to the other conglomerate bodies of the Antognola Formation and was quarried for aggregates in the past (Bonsignore et al., 1969). Clasts are not easily separated from the surrounding matrix as fractures commonly propagate straight across the clast/matrix boundary (Fig. 2b). When separated from the matrix, the clasts appear coated by a very thin film of dark green (almost blackish), fine-grained material.

The BPC is cut by fractures, up to a few mm thick, filled with very finely crystalline, whitish magnesite (determined by micro-Raman spectroscopy; see Supplementary File 2). These are likely related to late meteoric fluids, similarly to the dolomite and aragonite veinlets signalled in the BPC by Natale (1972), and will not be further discussed in this paper.

4.2. Peridotite clasts

Peridotite (lherzolite) clasts are generally rounded and pebble- to cobble-sized; they invariably show the following concentric zoning (Fig. 2c, d; 3a):

- a core made up of fresh lherzolite with the typical olive green colour;
- an internal rim (rim2), 10–30 mm thick, consisting of altered peridotite showing a brown-orange colour;
- an external rim (rim1), 4–12 mm thick, made up of dark green to blackish serpentinite, showing textural relics of the original peridotite.

The thickness of rim1 and rim2 is rather constant and independent from the diameter of the clast. For this reason, pebbles smaller than 3–4 cm in diameter do not generally show a fresh peridotite core, and in those smaller than 1–2 cm no zoning is present. No apparent erosion or breakage of serpentinized outer rims was observed.

The clast core consists of a lherzolite with relatively fresh olivine, clinopyroxene and orthopyroxene (Fig. 3a, b, c). The olivine is commonly fractured and shows an incipient alteration to brownish products along the fracture edges. Ameboid-shaped spinel crystals also occur, commonly rimmed by Mg-chlorite, as well as altered, ameboid-shaped plagioclase crystals.

In the intermediate rim2 (Fig. 3a, c, d), clinopyroxene crystals are commonly preserved. Conversely, all the olivine, as well as a large part of orthopyroxene crystals, are replaced by a brown-coloured, fine grained, low-birefringence material, unresolvable by optical microscopy and yelding no micro-Raman spectra due to fluorescence interference. XRPD indicates that this material is a mixture of serpentine (lizardite) and montmorillonite (see Supplementary File 3).

The external rim1 (Fig. 3a, e, f) consists of a lizardite serpentinite, pale green to pale brown in thin section. The olivine is completely serpentinized and the orthopyroxene is very rarely preserved, whereas non-serpentinized clinopyroxene crystals are still present. Lizardite replacement gives rise to mesh structures on former olivine and pseudomorphs after former pyroxenes (Fig. 3f). A representative micro-Raman spectrum of rim1 lizardite is shown in Fig. 4a. SEM-EDS analyses show that rim1 lizardite is free of Al_2O_3 and has a FeO (total Fe) content between 7.52 and 12.70 wt% (mean 10.46 wt%; 7 points).

The same concentric zoning is also superimposed to clasts of peridotite, which had already undergone partial, metamorphic serpentinization prior to clast formation and rounding. This consists of seams/bands of antigorite serpentinite that cross the peridotite and are sharply cut at clast edges. Peridotite clasts locally host veins made up of chrysotile±magnetite, also commonly observed in serpentinite clasts. Sharp truncation of these veins at clast edges, and their random orientation in adjoining clasts indicate that the opening of the veins predated the formation of the clasts.

4.2. Conglomerate matrix and cements

The BPC matrix is a poorly sorted lithic arenite made up of medium-grained to micro-conglomeratic, angular to subrounded grains whose composition reflects that of the conglomerate clasts, being mostly composed of serpentinite. The BPC is cemented by:

-cem1: 20–60 μm thick lizardite rim (Fig. 5a-f), corresponding to the thin film of dark coloured material coating the conglomerate clasts. Lizardite shows a yellowish colour and forms rosette-like aggregates composed of several-μm-sized flakes (Fig. 5f, g); these aggregates are arranged in a continuous, botryoidal rim. A representative micro-Raman spectrum of cem1 lizardite is shown in Fig. 4b. SEM-EDS analyses show that cem1 lizardite has a low Al_2O_3 content (0.61–2.29 wt%; mean 1.41 wt%; 17 points) and a FeO (total Fe) content between 2.83 and 9.60 wt% (mean 5.27 wt%; 17 points).

-cem2: 20–40 μm-sized scalenohedral calcite crystals. They form a nearly continuous rim in some samples, whereas in others only isolated calcite crystals are locally present. Cem2 is

composed of 96–99 mol% $CaCO_3$, below detection limit (bdl)–2 mol% $MgCO_3$, bdl–1.7 mol% $MnCO_3$, and bdl–0.7 mol% $FeCO_3$. Cem2 grows on a first layer of cem1 lizardite, a few μm thick, and is followed by a second layer of it (Fig. 5c, d). Where not completely coated by cem1, cem2 crystals serve as nuclei for the growth of cem3 carbonate (Fig. 5f).

-cem3: large, zoned crystals showing a first growth zone, 100–300 μm thick, composed of alternating bands with Ca-dolomite to high-Mg calcite composition (cem3a: 52.8–81.6 mol% $CaCO_3$, 17.9–46.2 mol% $MgCO_3$, bdl–3.3 mol% $MnCO_3$, and bdl–1.6 mol% $FeCO_3$), and a second, homogeneous growth zone of high-Mg calcite (cem3b: around 20 mol% $MgCO_3$; Fe and Mn bdl) plugging the remaining pore spaces (Fig. 5e, f).

5. Discussion and Conclusions

The peculiar internal structure of the BPC peridotite clasts, characterised by an isopachous serpentinized external rim (rim1), indicates that serpentinization occurred after the complete formation and rounding of the clasts. The constant thickness of the serpentinized rim1, which is independent from the clast diameter, and the absence of any evidence of transport post-dating serpentinization (e.g., erosion or breakage of rim1) indicates that serpentinization was post-depositional and occurred during the BPC diagenesis. The same considerations apply to the intermediate rim2. Fig. 6 provides a summary of the inferred relationships among primary (i.e., magmatic or metamorphic minerals preceding clast formation) and diagenetic minerals in the BPC.

The structures observed in BPC peridotite clasts closely resemble those reported by Cashman and Whetten (1976) in peridotite pebbles of Paleocene(?) alluvial fan conglomerates from Chiwaukum Graben (NE USA). The analogies include the presence of an outer rim composed of lizardite serpentinite, the preservation of the peridotite minerals in clast cores, and the lack of evidence for post-serpentinization transport. These authors interpreted lizardite rims as related to post-depositional serpentinization and claimed that it had probably occurred at less than 100°C, even though they could not precisely constraint the maximum burial reached by the studied conglomerate.

Conversely, the well-documented tectono-sedimentary evolution of the TH gives precise constraints to the BPC burial history. After deposition, the BPC was buried under Miocene–Pliocene marine sediments until eventual emersion and subaerial erosion of the TH relief system around the Pliocene–Pleistocene boundary (Festa et al., 2009, with refs.) Considering the cumulative thickness of the overlying Miocene-Pliocene units, the maximum burial depth reached by the BPC is estimated at 1400–1500 metres. This corresponds to a maximum diagenetic temperature of 50–60°C, considering a normal geothermal gradient of 25–30°C/km and a mean surface temperature of 15 °C. Moreover, the absence of marine cements predating the lizardite cement, and the moderate compaction observed in the BPC arenite matrix, suggest that the serpentinization and the associated precipitation of lizardite cement took place early after the deposition of the BPC, and thus at even lower temperatures than the maximum temperatures reached during burial.

Rim1 serpentinization resulted in the growth of lizardite which mimically grew on primary peridotite minerals, giving rise to mesh structure on olivine and pseudomorphs after pyroxenes. Rim1 lizardite is free of Al_2O_3 and has around 10% wt FeO (total Fe). Fe-rich lizardite with a similar iron content was documented by Evans et al (2009), and put in relation with a magnetite-free serpentinization process at low temperature. This is consistent with the inferred context of lizardite formation in the BPC, and matches the observed absence of magnetite in rim1 lizardite.

In rim2, the olivine and a part of the pyroxenes are replaced by lizardite and montmorillonite; rim2 shows a greater preservation of pyroxenes with respect to rim1. This, and the position between rim1 and the preserved peridotite core, seems to indicate that rim2 records an intermediate degree of peridotite alteration with respect to rim1, even if it is not possible to establish the relative chronology and the parameters controlling the formation of diagenetic mineral assemblages in rim1 and rim2.

The diagenetic nature of the serpentinization of BPC peridotite clasts is further supported by the occurrence of a rim of lizardite cement (cem1) surrounding the BPC clasts. This cement,

indeed, likely derives from Mg and Si released during non-isochemical serpentinization (cf. Pinto et al., 2015; 2017) of the external rim1 of peridotite clasts. Fe- and Al-rich minerals of the serpentine group (berthierine and odinite) occur as both cements and replacement phases in marine sediments of different ages (e.g., Van Houten and Purucker, 1984; Odin, 1988; Young and Taylor, 1989). Conversely, this is the first reported case of lizardite serving as a cement in a sedimentary rock, and, more generally, one of the first cases for a serpentine, the diagenetic growth of chrysotile cement having been documented within Holocene subaerial debris flow deposits rich in serpentinite clasts from New Zealand (Craw et al., 1987; 1995).

Pores in the BPC matrix are plugged by Mn- and Fe-bearing Ca-dolomite and high-Mg calcite cements. Carbonate precipitation was possibly induced by alkaline conditions created in the pore fluids by the serpentinization of the peridotite clasts, also representing a possible source of Mg, Mn and Fe. Carbonate precipitation promoted by serpentinization-derived alkaline fluids is indeed largely documented within ultramafic rocks in present-day examples, both from oceanic (e.g., Früh-Green et al., 2003; Ludwig et al., 2006) and continental settings (e.g., Bruni et al., 2002; Chavagnac et al., 2013; Giampouras et al., 2019); carbonate precipitation from seeping of serpentinization-derived fluids was also recently reported in ancient shallow-marine clastic sediments overlying the Semail Ophiolite in Oman (Eickmann et al., 2021). A link between serpentinization of BPC peridotite clasts and precipitation of carbonate cements is also suggested by the anomalous, high cementation of the BPC, which is far more cemented with respect to the surrounding sedimentary deposits.

Even though further investigation is needed to constrain the timing and the physical-chemical conditions underlying the formation of BPC diagenetic lizardite, the preliminary field and petrographic observations and the well-constrained burial history of BPC indisputably indicate that lizardite formed in diagenetic conditions at a burial depth not exceeding 1500 m, and under a temperature not higher than 50–60°C. This is the first reported case of very low *T* (<<100°C) serpentinization in a non-oceanic, non-ophiolitic setting, and the full

comprehension of its mechanisms can provide useful insights into low-*T* serpentinization processes.

The BPC case also shows that diagenetic serpentinization can promote strong cementation of peridotite-clast-rich sedimentary bodies in otherwise poorly cemented sedimentary successions. Moreover, the possibility of post-depositional serpentinization of peridotite clasts has to be taken into account when compositional analysis of terrigenous rocks composed of (meta-)ophiolite clasts is performed. In fact, because of diagenetic serpentinization, the presence and abundance of un-serpentinised peridotite clasts in the original sediments could be overlooked or pass completely unnoticed, especially where clasts larger than a few centimetres (thus capable to preserve an unaltered peridotite core) are absent.

Acknowledgements

SB's scholarship and JRP's postdoctoral fellowship were funded by the INAIL - BRIC 2019 project (grant number ID 57.1). Micro-Raman spectra have been obtained with the equipment acquired by the Interdepartmental Centre "G. Scansetti" for Studies on Asbestos and Other Toxic Particulates (University of Torino) with a grant from Compagnia di San Paolo, Torino, Italy. The authors thank Roberto Compagnoni for the fruitful discussions and suggestions.

References

Agrinier, P., Cornen, G. , Beslier, M.O., 1996. Mineralogical and oxygen isotope features of serpentinites recovered from the ocean/continent transition in the Iberia Abyssal Plain. Proceedings of the Ocean Drilling Program, Scientific Results 149, 541–552.

Barnes, I., O'Neil, J.R.,Trescases, J.J., 1978. Present day serpentinization in New Caledonia, Oman and Yugoslavia. Geochim. Cosmochim. Acta 42(1), 144–145.

Bonsignore, G., Bortolami, G., Elter, G., Montrasio, A., Petrucci, F., Ragni, U., Sacchi, R., Sturani, C., Zanella, E., 1969. Note Illustrative della Carta Geologica d'Italia alla scala 1: 100.000. Fogli 56 e 57 Torino–Vercelli. Poligrafica & Cartevalori, Ercolano (NA).

Bruni, J., Canepa, M., Chiodini, G., Cioni, R., Cipolli, F., Longinelli, A., Marini, L., Ottonello, G., Vetuschi Zuccolini, M., 2002. Irreversible water–rock mass transfer accompanying the generation of the neutral, Mg–HCO_3 and high-pH, Ca–OH spring waters of the Genova province, Italy. Applied Geochem. 17 (4), 455–474.

Cannat, M., Fontaine, F., Escartín, J., 2010. Serpentinization and Associated Hydrogen And Methane Fluxes at Slow Spreading Ridges. In: P.A. Rona, C.W. Devey, J. Dyment, B.J. Murton (Eds.) Diversity Of Hydrothermal Systems On Slow Spreading Ocean Ridges. AGU Geophysical Monograph 188, pp. 241–264.

Cashman, S.M., Whetten, J.T., 1976. Low-temperature serpentinization of peridotite fanglomerate on the west margin of the Chiwaukum graben, Washington. GSA Bull. 87 (12), 1773–1776.

Chavagnac, V., Ceuleneer, G., Monnin, C., Lansac, B., Hoareau, G., Boulart, C., 2013. Mineralogical assemblages forming at hyperalkaline warm springs hosted on ultramafic rocks: A case study of Oman and Ligurian ophiolites. Geochem. Geophys. Geosyst. 14, 2474–2495.

Compagnoni, R., Forno, M.G., 1992. Significato geologico di depositi fluviali ghiaiosi pleistocenici medi nella Collina di Torino. Il Quaternario 5(1), 105–122.

Compagnoni, R., Cossio, R., Mellini, M., 2021. Raman anisotropy in serpentine minerals, with a caveat on identification. J. Raman Spectrosc. 52, 1334– 1345.

Craw, D., Landis, C.A., Kelsey, P.I., 1987. Authigenic chrysotile formation in the matrix of Quaternary debris flows, Northern Southland, New Zealand. Clays Clay Min. 35, 43–52.

Craw, D., Blattner, P., Landis, C., 1995. Stable isotopic signatures of authigenic minerals in a Holocene ophiolitic debris flow, Southland, New Zealand. Clay Min. 30(2), 165–172.

Eickmann, B., Little, C.T.S., Peckmann, J., Taylor, P.D., Boyce, A.J., Morgan, D.J., Bach, W., 2021. Shallow-marine serpentinization-derived fluid seepage in the Upper Cretaceous Qahlah Formation, United Arab Emirates. Geol. Mag. 158 (9), 1561–1571.

Elter, G., Elter, P., Sturani, C., Weidmann, M., 1966. Sur la prolongation du Domaine Ligure de l'Apennin dans le Monferrat et les Alpes et sur l'origine de la nappe de la Simme s.l. des Préalpes Romandes et Chablaisiennes. Arch. Sci. Genève 19 (3), 279–377.

Etiope, G., 2017. Abiotic methane in continental serpentinization sites: an overview. Procedia Earth Planet. Sci. 17, 9–12.

Evans, B.W., 2004. The serpentinite multisystem revisited: chrysotile is metastable. Int. Geol. Rev. 46 (6), 479–506.

Evans, B.W., Kuehner, S.M., Chopelas, A., 2009. Magnetite-free, yellow lizardite serpentinization of olivine websterite, Canyon Mountain complex, N.E. Oregon. American Mineralogist 94 (11-12), 1731–1734.

Festa, A., Boano, P., Irace, A., Lucchesi, S., Forno, M. G., Dela Pierre, F., Fioraso, G., Piana, F., 2009. Carta Geologica d'Italia alla scala 1:50.000. Foglio 156 Torino Est. APAT, Agenzia per la Protezione dell'Ambiente e per i Servizi Tecnici - Dipartimento Difesa del Suolo, Roma.

Fryer, P., Mottl, M.J., 1992. Lithology, mineralogy, and origin of serpentine muds recovered from Conical and Torishima forearc seamounts: results of Leg 125 drilling. Proceedings of the Ocean Drilling Program, Scientific Results 125, 343–362.

Früh-Green, G.L., Kelley, D.S., Bernasconi, S.M., Karson, J.A., Ludwig, K.A., Butterfield, D.A., Boschi, C., Proskurowski, G., 2003. 30,000 years of hydrothermal activity at the Lost City vent field. Science 301, 495–8.

Früh-Green, G.L., Connolly, J.A.D., Plas, A., Kelley, D.S., Grobéty, B., 2004. Serpentinization of Oceanic Peridotites: implications for geochemical cycles and biological activity. In: W.S. Wilcock, E.F. Delong, D.S. Kelley, J.A. Baross, S. Craig Cary (eds.) The Subseafloor Biosphere at Mid-Ocean Ridges. Geophysical Monograph Series 144, pp.119–136.

Giampouras, M., Garrido, C.J., Zwicker, J., Vadillo, I., Smrzka, D., Bach, W., Peckmann, J., Jiménez, P., Benavente, J., García-Ruiz, J.M., 2019. Geochemistry and mineralogy of serpentinization-driven hyperalkaline springs in the Ronda peridotites. Lithos 350–351, 105215.

Guillot, S., Hattori, K., 2013. Serpentinites: essential roles in geodynamics, arc volcanism, sustainable development, and the origin of life. Elements 9(2), 95–98.

Ludwig, K.A., Kelley, D.S., Butterfield, D.A., Nelson, B.K., Früh-Green, G., 2006. Formation and evolution of carbonate chimneys at the Lost City hydrothermal field. Geochim. Cosmochim. Acta 70, 3625–3645.

Natale, P., 1972. Nuove osservazioni sull'origine dei giacimenti di magnesite delle Alpi Occidentali. Bollettino dell'Associazione Mineraria Subalpina, 9(1-2), 107–124.

Odin, G.S., 1988. Green Marine Clays. Developments in Sedimentology Series, 45. Elsevier, Amsterdam.

Petriglieri, J.R., Salvioli-Mariani, E., Mantovani, L., Tribaudino, M., Lottici, P.P., Laporte-Magoni, C., Bersani, D., 2015. Micro-Raman mapping of the polymorphs of serpentine. J. Raman Spectrosc. 46, 953–958.

Piana, F., Fioraso, G., Irace, A., Mosca, P., d'Atri, A., Barale, L., Falletti, P., Monegato, G., Morelli, M., Tallone, S., Vigna, G.B., 2017. Geology of Piemonte region (NW Italy, Alps-Apennines interference zone). J. Maps 13, 395–405.

Pinto, V.H.G., Manatschal, G., Karpoff, A.M., Viana, A.R., 2015. Tracing mantle-reacted fluids in magma-poor rifted margins: The example of Alpine Tethyan rifted margins. Geochem. Geophys. Geosyst. 16, 3271–3308.

Pinto, V.H.G., Manatschal, G., Karpoff, A.M., Ulrich, M., Viana, A.R., 2017. Seawater storage and element transfer associated with mantle serpentinization in magma-poor rifted margins: A quantitative approach. Earth Planet. Sci. Letters 459, 227-237.

Polino, R., Ruffini, R., Ricci, B., 1991. Le molasse terziarie della Collina di Torino: relazioni con la cinematica alpina. Atti Ticinensi di Scienze della Terra 34(Note Brevi), 85–95.

Rinaudo, C., Gastaldi, D., Belluso, E., 2003. Characterization of chrysotile, antigorite and lizardite by FT-Raman spectroscopy. Canad. Mineralogist 41, 883–890.

Sacco, F., 1936. Il fenomeno diluvio-glaciale nelle Alpi durante l'Era terziaria. Boll. Soc. Geol. It. 55(1), 63–115.

Sánchez-Murillo, R., Gazel, E. , Schwarzenbach, E., Crespo-Medina, M., Schrenk, M.O., Boll, J., Gill, B.C., 2014.) Geochemical evidence for active tropical serpentinization in the Santa Elena Ophiolite, Costa Rica: An analog of a humid early Earth? Geochem. Geophys. Geosyst. 15, 1783–1800.

Schrenk, M.O., Brazelton, W.J., Lang, S.Q., 2013. Serpentinization, Carbon, and Deep Life. Rev. Mineral. Geochem. 75 (1), 575–606.

Van Houten, F.B., Purucker, M.E., 1984. Glauconitic peloids and chamositic ooids - favorable factors, constraints, and problems. Earth-Sci. Rev. 20 (3), 211–243.

Young, T.P., Taylor, W.E.G., 1989. Phanerozoic Ironstones. Geological Society of London, Special Publication 46. The Geological Society, London.

Figures

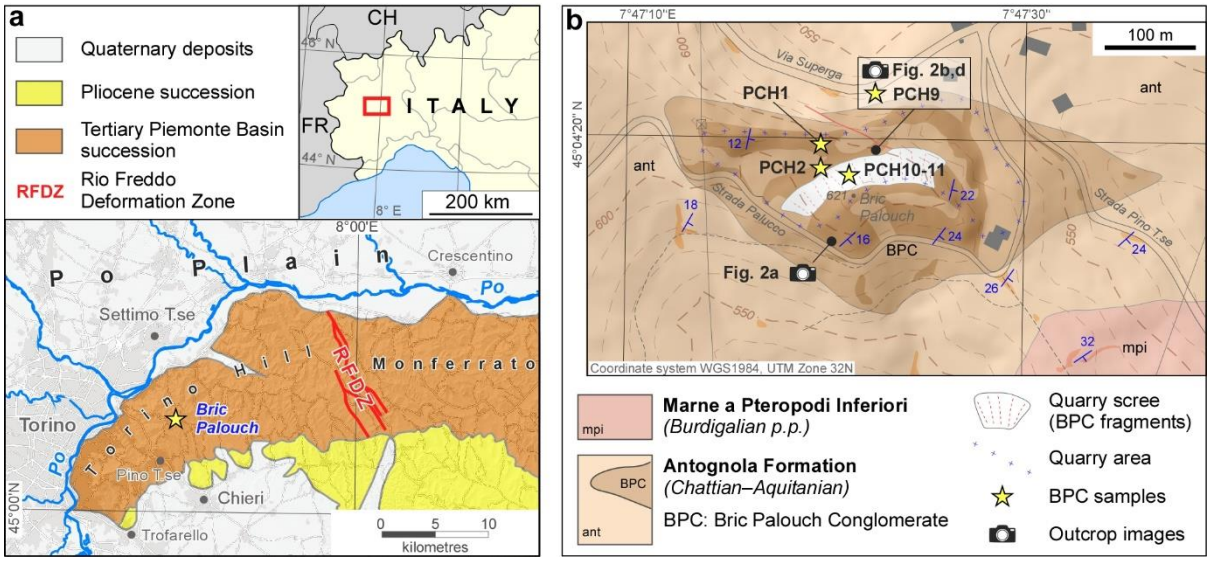

Fig.1. a) Geological scheme showing the position of the Bric Palouch Conglomerate in the Torino Hill. **b)** Geological map of the Bric Palouch Conglomerate, showing the position of the sampling points and of the outcrops figured in this paper. *Figure width: 2 columns*

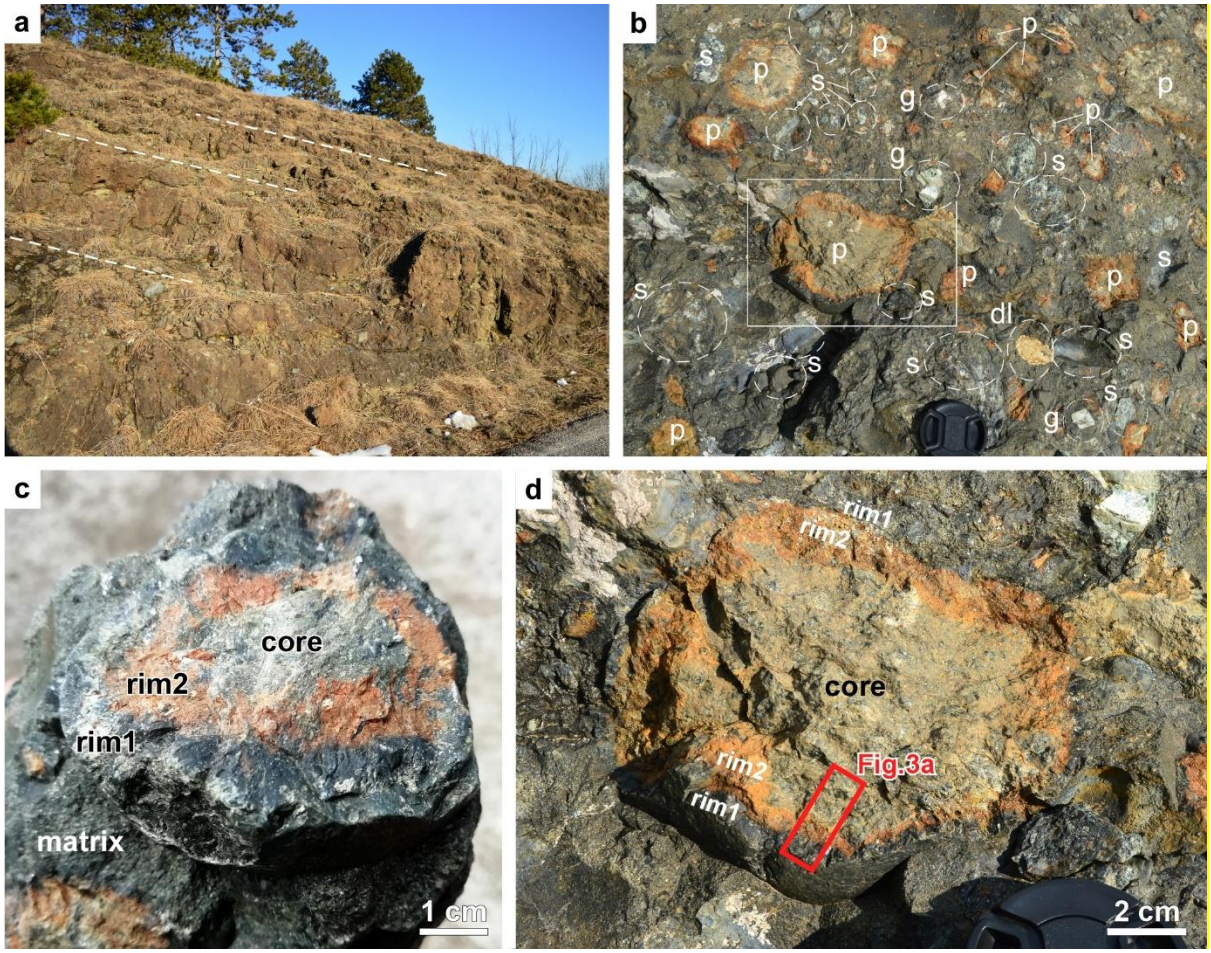

Fig.2. Field images of the Bric Palouch Conglomerate (BPC). **a)** Roadside exposure of BPC, showing reddish brown weathered surfaces and an ill-defined, metre-thick bedding (dashed lines; coordinates: 45°04'16.1"N; 7°47'20.5"E). **b)** Fresh surface of BPC exposed in the Bric Palouch quarry (coordinates 45°04'19.4"N; 7°47'22.2"E), showing rounded clasts of peridotite (p), serpentinite (s), metagabbro (g), and dolomitic limestone (d). Most of the serpentinite clasts are indistinguishable from the matrix as they show a similar colour. Note the dark, serpentinized rim around peridotite clasts. The rectangle shows the area enlarged in d). Lens cap for scale is 52 mm across. **c, d)** Peridotite pebble (c, sample PCH2) and cobble (d, sample PCH9) showing a clear zoning defined by an outer, dark-coloured serpentinized rim (rim1), an inner, orange-coloured, altered peridotite rim (rim2), and a fresh peridotite core. Note that in d), the distinction of the serpentinized rim1 from the conglomerate matrix is difficult where the clast is still encased in the matrix (upper part of the image). The red rectangle in d) indicates the area corresponding to the photomicrograph mosaic of Fig. 3a. *Figure width: 2 columns*

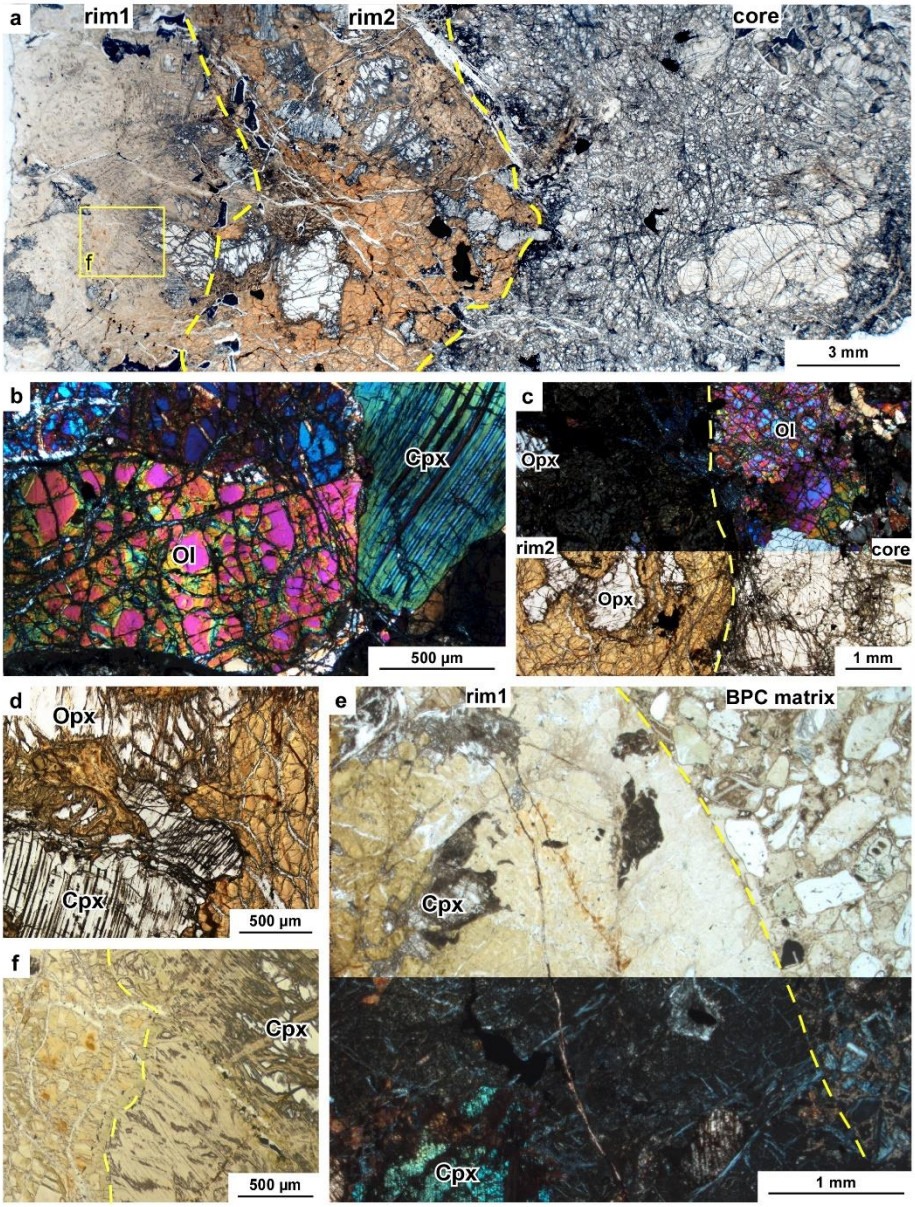

Fig.3. BPC peridotite clasts (a–d, f: sample PCH9; e: sample PCH2). **a)** Micro-photomosaic (plane polarised light: PPL) of the outer portion of a peridotite cobble, corresponding to the red rectangle in Fig. 2d, showing sharp passages between the serpentinized rim1 and rim2 and between rim2 and the fresh peridotite core. The yellow rectangle indicates the area shown in f). **b)** Fresh peridotite core, with preserved olivine (Ol) and clinopyroxene (Cpx) (PPL). **c)** Passage between fresh peridotite core and rim2 with preserved orthopyroxene crystals (Opx) (top, cross polarised light: CPL; bottom, PPL). **d)** Detail of rim2, with serpentinized olivine (brown) and preserved clinopyroxene (Cpx) and orthopyroxene (Opx) (PPL). **e)** Pale-green, serpentinized rim1 of a peridotite pebble with preserved clinopyroxenes (Cpx) (top, PPL; bottom, CPL). **f)** Detail of the serpentinized rim1 of a peridotite cobble; lizardite gives rise to mesh structure after olivine (left) and pseudomorphs after clinopyroxene (right), partly preserved in the upper right corner (Cpx) (PPL). *Figure width: 2 columns*

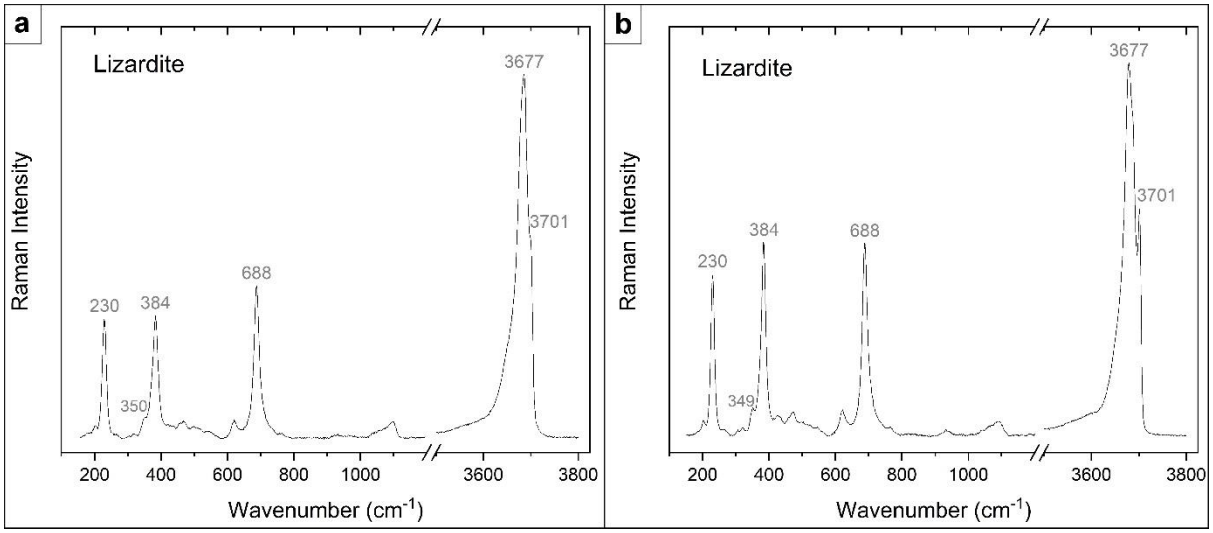

Fig.4. Representative micro-Raman spectra. **a)** Lizardite from serpentinized rim1 of a peridotite pebble (sample PCH10). **b)** Lizardite cement (cem1, sample PCH10). Raman spectra were deconvoluted for a more reliable attribution of characteristic Raman peaks. *Figure width: 2 columns*

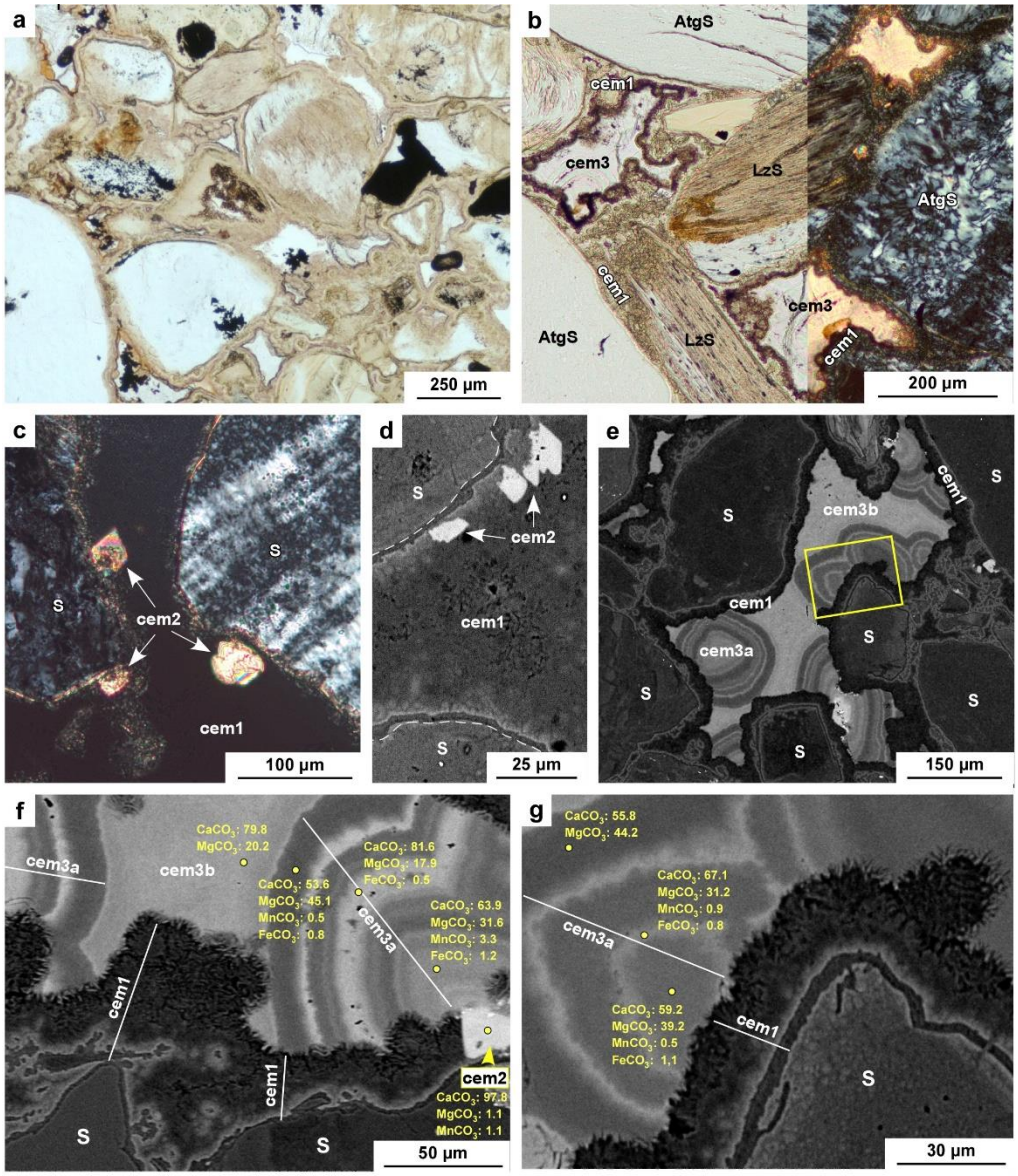

Fig.5. BPC arenite matrix in thin section (a–c, e–g: sample PCH10; d: sample PCH2). **a)** BPC arenite matrix; the serpentinite grains are coated by an isopachous, pale-green lizardite cement rim; the remaining voids are plugged by carbonate cement (PPL). **b)** Detail of the lizardite cem1 rim, showing a botryoidal aspect and growing on both antigorite serpentinite (AtgS) and lizardite serpentinite (LzS) grains; the pores are plugged by cem3 carbonate (left, PPL; right, CPL). **c, d)** Serpentinite grains (S) coated by cem1 lizardite cement; isolated cem2 scalenohedral calcite crystals grow on a thin rim of cem1 and are coated by the further growth of cem1 (c, CPL; d, SEM-BSE). **e)** Large pore among serpentinite grains (S), coated by a rim of cem1 lizardite and plugged by cem3 carbonate; the yellow rectangle indicates the area enlarged in g) (SEM-BSE). **f, g)** Details of pore cements growing on serpentinite grains (S); in f), note how cem2 calcite serves as nucleus for the subsequent growth of cem3a Mg-rich carbonate (SEM–BSE). The yellow points on carbonate cements indicate the spots of EDS analyses (calculated compositions are in mol%). *Figure width: 2 columns*

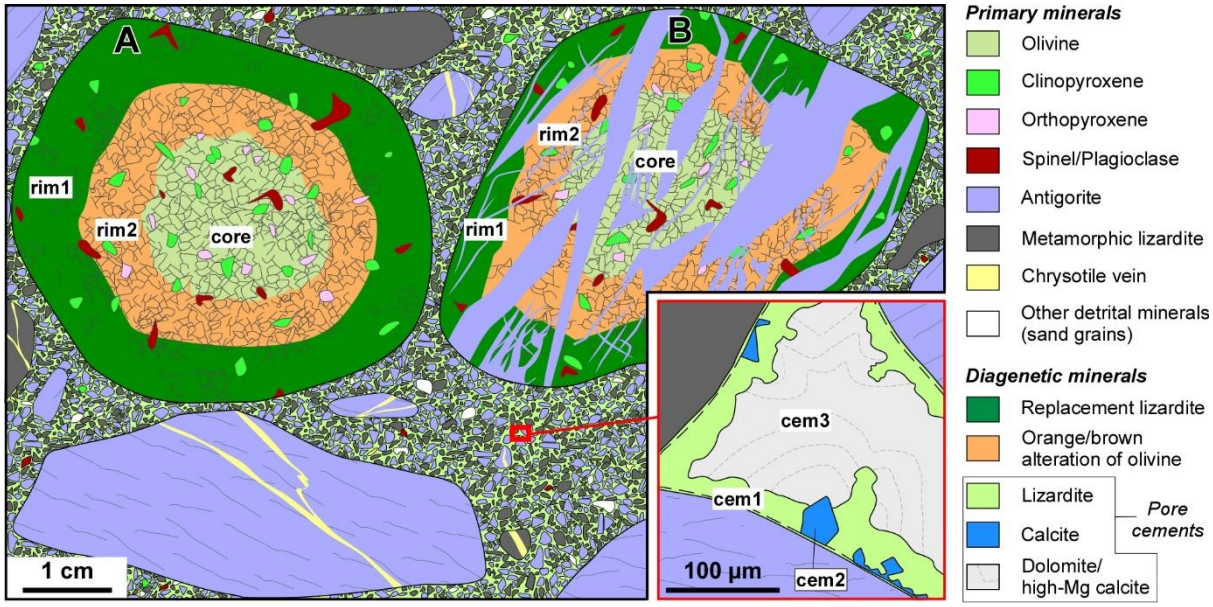

Fig.6. Interpretative sketch showing the observed petrographic characters of the BPC. Distinction is made between primary minerals (i.e., magmatic or metamorphic) and diagenetic minerals. Pebble labelled ‘A' shows a fresh peridotite core and serpentinized rim1 and rim2. In pebble ‘B’, the diagenetic serpentinization (rim1 and rim2) was superimposed on a peridotite pebble which had already suffered a partial, metamorphic antigorite serpentinization. In the arenite matrix, all the lizardite serpentinite grains are indicated as “metamorphic lizardite”, even though a part of them may be the result of diagenetic serpentinization of peridotite grains. The inset shows the observed relationships between the pore cements. *Figure width: 2 columns*